Supplementary Fig. 1

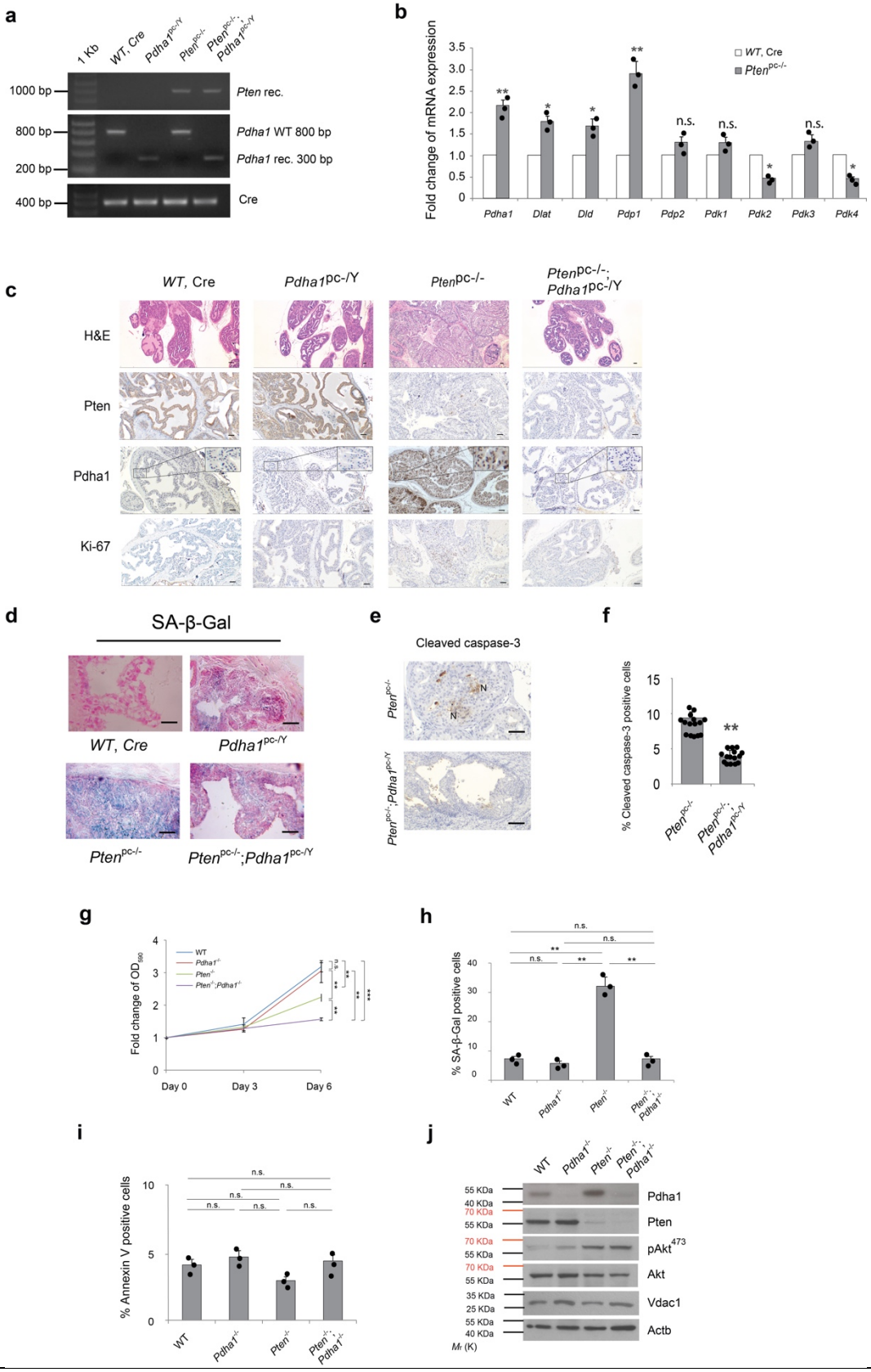

Supplementary Figure 1

Pdha1 knockout induces tumour suppression in mice prostate tumours.

(**a**) The efficiency of *Probasin-Cre4 (Pb-Cre4)* mediated recombination of the *Pten*$^{loxP/loxP}$ and *Pdha1*$^{loxP/Y}$ allele as scored by PCR amplification in wild type, *Pdha1*$^{pc-/Y}$, *Pten*$^{pc-/-}$ and *Pten*$^{pc-/-}$; *Pdha1*$^{pc-/Y}$ prostates and tumours. (n=3, independent prostate samples) (**b**) Quantitative real time-PCR analysis of mRNA expression of *Pdha1, Dlat, Dld* and Pdha1 regulator genes in *Pten*$^{pc-/-}$ prostate tumours versus wild type prostate tissues (n=3, independent prostate samples)**. (c-d**) Representative micrographs in histopathological analysis (haematoxylin/eosin staining and indicated proteins) of anterior prostates (AP) (n=3, independent prostate samples, 5 fields for each group, scale bar represents 50 μm) (**c**) and representative micrographs of senescence associated β-Gal (SA- β-Gal) staining (n=3 independent prostate samples, 5 fields for each group and scale bar represents 50 μm) (**d**) in wild type, *Pdha1*$^{pc-/Y}$, *Pten*$^{pc-/-}$ and *Pten*$^{pc-/-}$; *Pdha1*$^{pc-/Y}$ prostates and tumours. (**e, f**) Apoptosis analysis by cleaved caspase 3 (**e**) and quantification of the percentage of cleaved caspase 3 positive cells (**f**) of anterior prostates (AP) in 12-week-old *Pten*$^{pc-/-}$ and *Pten*$^{pc-/-}$; *Pdha1*$^{pc-/Y}$ tumours (N: small necrotic foci, n=3 mice, 5 fields for each group and scale bar represents 50 μm). (**g-j)** Relative cell number quantification by crystal violet staining (**g**), senescence associated β-Gal (SA-β-Gal) staining (**h**), cellular apoptosis assay by Annexin V staining (**i**) and western blot analysis of indicated proteins (**j**) of wild type, *Pdha1*$^{-/-}$, *Pten*$^{-/-}$ and *Pten*$^{-/-}$; *Pdha1*$^{-/-}$ MEFs on 6th day after retroviral Cre infection and selection. Uncropped images are in Supplementary Figure 13. (n=3, independent cell cultures). Error bars indicate s.e.m. **P* < 0.05; ***P* < 0.01. n.s, not significant.

Supplementary Fig. 2

a

	Primary vs normal		Metastasis vs primary		Metastasis vs normal	
	DNA	mRNA	DNA	mRNA	DNA	mRNA
	Significantly amplified	Significantly overexpressed	Significantly amplified	Significantly overexpressed	Significantly amplified	Significantly overexpressed
PDHA1	1 out of 3 datasets	3 out of 17 datasets	2 out of 3 datasets	7 out of 13 datasets	1 out of 1 datasets	no probe
PDP1	3 out of 3 datasets	9 out of 11 datasets	3 out of 3 datasets	1 out 9 datasets	1 out of 1 datasets	no probe

b

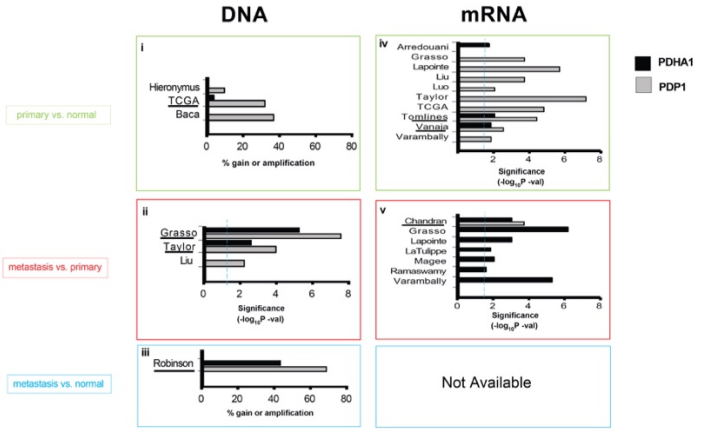

c

DNA

i, Primary vs normal germline

Study	PDHA1 Total sample number	PDHA1 % samples with aberration	PDP1 Total sample number	PDP1 % samples with aberration
Hieronymus	104 vs 104	0% gain or amp	104 vs 104	9% gain or amp
TCGA	492 vs 492	4% gain or amp	492 vs 492	32% gain or amp
	492 vs 492	5% hetloss or homdel	492 vs 492	2% hetloss or homdel
Baca	57 vs 57	0% gain or amp	57 vs 57	37% gain or amp
	57 vs 57	0% gain or amp	57 vs 57	0% hetloss or homdel

ii, Metastasis vs primary

Study	PDHA1 Sample number	PDHA1 p-val[1]	PDP1 Sample number	PDP1 p-val[1]
Grasso	35 vs 59	0.0000049	35 vs 59	0.0000049
Taylor	37 vs 161	0.003	37 vs 161	0.00011
Liu	55 vs 3	ns	55 vs 3	0.006

iii, Metastasis vs normal germline

Study	Total sample number	% samples with aberration	Total sample number	% samples with aberration
Robinson	150 vs 150	43% gain or amp	150 vs 150	69% gain or amp
	151 vs 150	4% hetloss or homdel	151 vs 150	1% hetloss or homdel

1 ns: no probe, ns: non significant deregulation
2 In parenthesis: specific probe when discordant deregulation patterns between probes were found
red font: overexpression or gain/amplification of PDHA1 and/or PDP1; blue font: underexpression or loss of heterozygosity/homozygous deletion of PDHA1 and/or PDP1
grey background: same results for same gene in same comparison from the same study

mRNA

iv, Primary vs normal gland

Study	PDHA1 Sample number	PDHA1 p-val[1,2]	PDP1 Sample number	PDP1 p-val[1]
Arredouani	13 vs 8	0.018	13 vs 8	
Grasso	59 vs 28	ns	59 vs 28	0.00017
Lapointe	62 vs 41	ns	62 vs 41	0.0000018
LaTulippe	23 vs 3	0.000019	23 vs 3	np
Liu	44 vs 13	ns	44 vs 13	0.00018
Luo	15 vs 15	ns	15 vs 15	0.009
Taylor	131 vs 29	0.01	131 vs 29	0.000000057
TCGA	497 vs 52	ns	497 vs 52	0.000015
Tomlins	30 vs 23	0.009	30 vs 21	0.000035
Vanaja	27 vs 8	0.013	27 vs 8	0.003
Varambally	7 vs 6	0.019	7 vs 6	0.013

v, Metastasis vs primary

Study	PDHA1 Sample number	PDHA1 p-val[1,2]	PDP1 Sample number	PDP1 p-val[1]
Chandran	21 vs 10	0.00096 (GE79463)	21 vs 10	0.00018
	21 vs 10	0.000000077 (GE86300)		
Grasso	35 vs 59	0.00000062	35 vs 59	0.047
Taylor	19 vs 131	ns	19 vs 131	ns
Lapointe	9 vs 61	0.00085	9 vs 61	ns
LaTulippe	9 vs 23	0.016	9 vs 23	np
Magee	3 vs 8	0.009	3 vs 8	np
Ramaswamy	3 vs 10	0.047	3 vs 10	ns
Varambally	6 vs 7	0.0000047	6 vs 7	ns

Metastasis vs normal gland

Study	PDHA1 Sample number	PDP1 Sample number

Not Available

d

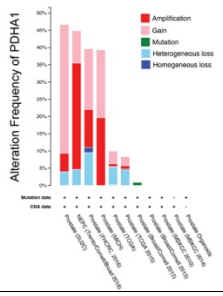

e

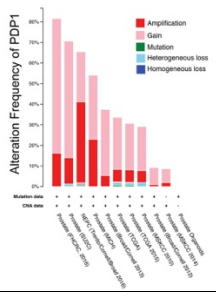

Supplementary Figure 2

***PDHA1* and *PDP1* get frequently amplified and overexpressed in human prostate cancer.**

(**a-c**) The number of datasets (**a**), bar graph of amplification or overexpression of these datasets and underlined are comparisons (7 out of 24) where both genes are gained/amplified or overexpressed (**b**) and sample number in indicated comparison and *P* value (**c**) from Oncomine or cBioPortal cohorts by which significant copy-number gain or amplifications (DNA) or overexpression (mRNA) exits when the following comparisons are computed: i, DNA, primary versus normal germline; ii, DNA, metastasis versus primary; iii, DNA, metastasis versus normal germline; iv, mRNA, primary versus normal prostate glands and v, mRNA, metastasis versus primary. Significant overexpression or copy number values are computed using T-test (two-tailed, $P<0.05$, in ii, iv and v), or using GISTIC or RAE (in i and iii). (**d,e**) Alteration frequency analysis of *PDHA1* (**d**) and *PDP1* (**e**) from 11 studies on prostate cancers available on cBioPortal.

Supplementary Fig. 3

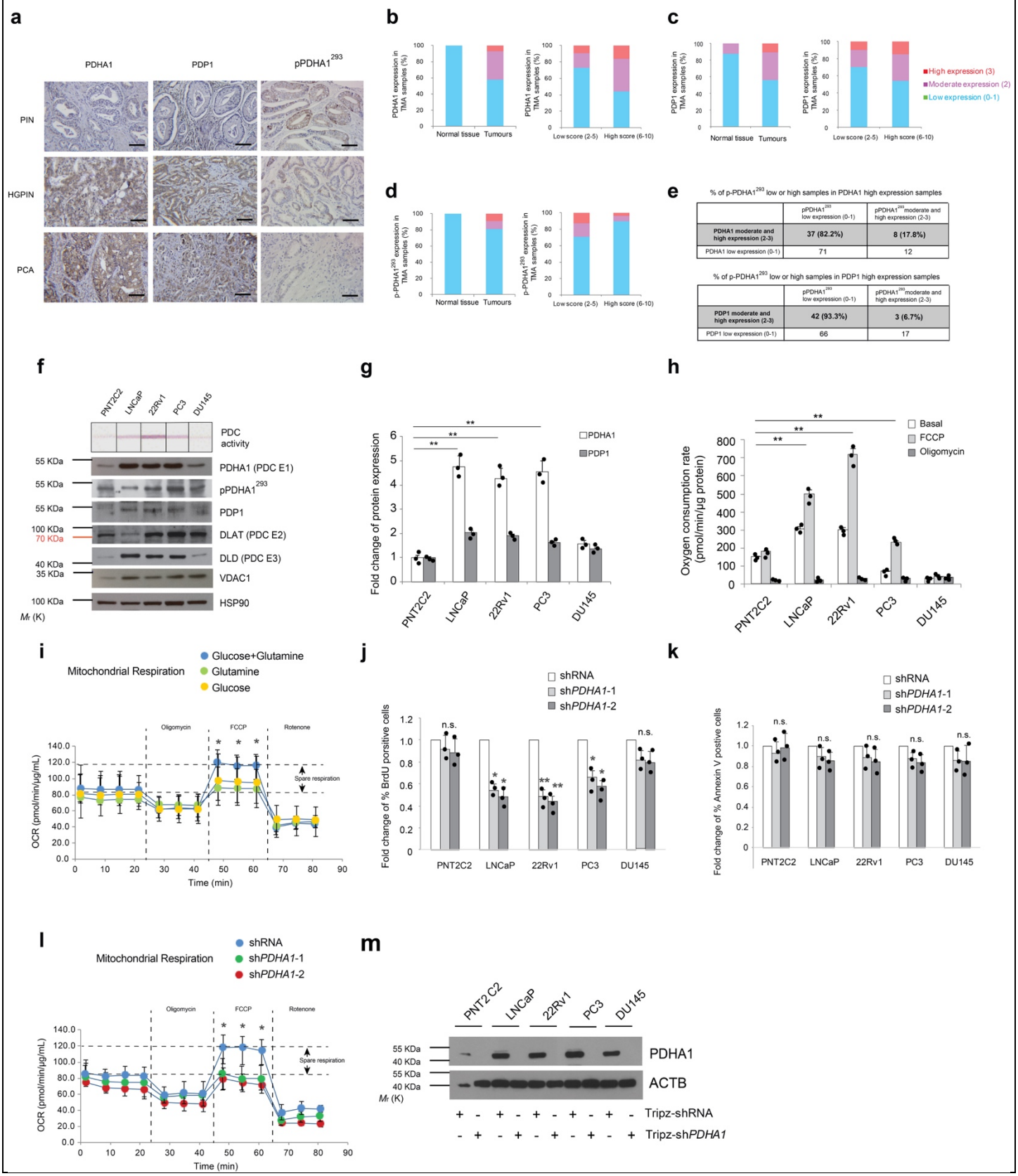

Supplementary Figure 3

PDHA1 and PDP1 get overexpressed in human prostate cancer cell lines and tumours.

(**a**) Representative immune-histochemical staining for PDHA1, phospho-PDHA1^{293} and PDP1 in a prostate cancer tissue microarray (TMA) of 128 patients (5 fields acquired for each sample, PIN indicates prostatic intraepithelial neoplasia, HGPIN indicates high-grade prostatic intraepithelial neoplasia, PCA indicates invasive prostate cancer, and scale bar represents 50 μm) (**b-d**) Evaluation and quantification of immune-histochemical staining for PDHA1 (**b**), PDP1 (**c**) and phospho-PDHA1^{293}(**d**) in human tumour samples in panel (**a**). (**e**) Quantification of immune-histochemical staining of phospho-PDHA1^{293} in PDHA1 or PDP1 moderate/high expression samples. The gray frames highlighted the numbers of PDHA1 or PDP1 moderate/high expression samples (**f**) Upper panel, PDC activity measurements in prostate cancer cells using a standard quantitative dipstick assay (n=3, independent cell cultures). Lower panel, western blot analysis of indicated proteins in prostate cancer cell lines. Uncropped images are in Supplementary Figure 14. (n=3, independent cell cultures). (**g**) Quantification of western blots for PDHA1 and PDP1 in panel (**f**) (n=3, independent cell cultures). (**h**) Mitochondrial oxygen consumption rate analysis of the indicated prostate cancer cell lines (n=3, independent cell cultures). (**i**) Mitochondrial oxygen consumption rate analysis of 22Rv1 prostate cancer cell line in the media supplemented with glucose (11 mM), glutamine (2 mM) or a combination of these two (n=3, independent cell cultures). (**j,k**) Cellular proliferation assay by BrdU staining (**j**) and cellular apoptosis assay by Annexin V staining (**k**) in cell lines infected with indicated sh*PDHA1* or scramble shRNA control (n=3, independent cell cultures). (**l**) Mitochondrial oxygen consumption rate analysis of 22Rv1 prostate cancer cell line infected with sh*PDHA1* or scramble control. (n=3, independent cell cultures). (**m**) Western blot analysis of PDHA1 in cell lines infected with doxycycline-induced Tripz-sh*PDHA1* or scramble control in Fig. 1 panel (**h-j**). Uncropped images are in Supplementary Figure 14. (n=3, independent cell cultures). Error bars indicate s.e.m. *$P < 0.05$; **$P < 0.01$. n.s, not significant.

Supplementary Fig. 4

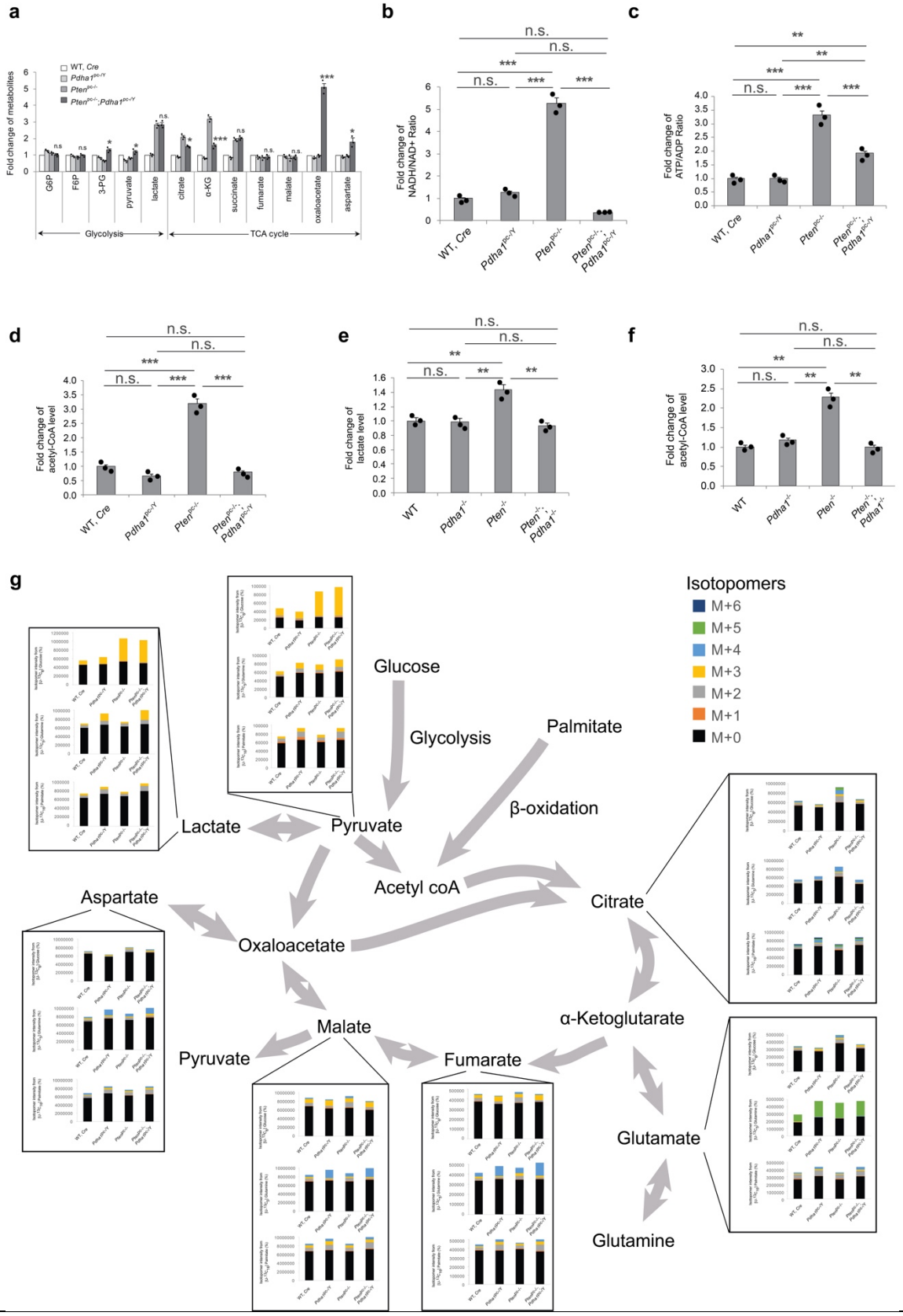

Supplementary Figure 4

Pdha1 inactivation decreases mitochondrial intermediates.

(**a**) Representative intermediates level in glycolysis and tricarboxylic acid (TCA) cycle of wild type, *Pdha1*$^{pc-/Y}$, *Pten*$^{pc-/-}$ and *Pten*$^{pc-/-}$; *Pdha1*$^{pc-/Y}$ prostates and tumours (n=3, independent prostate samples). (**b-d**) Determination of relative NADH/NAD^{+} ratio (**b**), ATP/ADP ratio (**c**) and acetyl coA levels (**d**) in wild type, *Pdha1*$^{pc-/Y}$, *Pten*$^{pc-/-}$ and *Pten*$^{pc-/-}$; *Pdha1*$^{pc-/Y}$ prostates and tumours (n=3, independent prostate samples). (**e,f**) Determination of extracellular lactate levels (**e**) and acetyl coA levels (**f**) in wild type, *Pdha1*$^{-/-}$, *Pten*$^{-/-}$ and *Pten*$^{-/-}$; *Pdha1*$^{-/-}$ MEFs (n=3, independent cell cultures). (**g**) Representative data depict abundance of selected labelled metabolites from [U-$^{13}C_6$]-Glucose, [U-$^{13}C_5$]-Glutamine and [U-$^{13}C_{16}$]-palmitate respectively in mouse prostate epithelial cells derived from wild type, *Pdha1*$^{pc-/Y}$, *Pten*$^{pc-/-}$ and *Pten*$^{pc-/-}$; *Pdha1*$^{pc-/Y}$ prostates and tumours. Glucose, glutamine and Palmitate metabolism profiles were presented as actual intensities. (n=3, independent prostate samples). Error bars indicate s.e.m. **P* < 0.05; ***P* < 0.01; ****P* < 0.001. n.s, not significant.

Supplementary Fig. 5

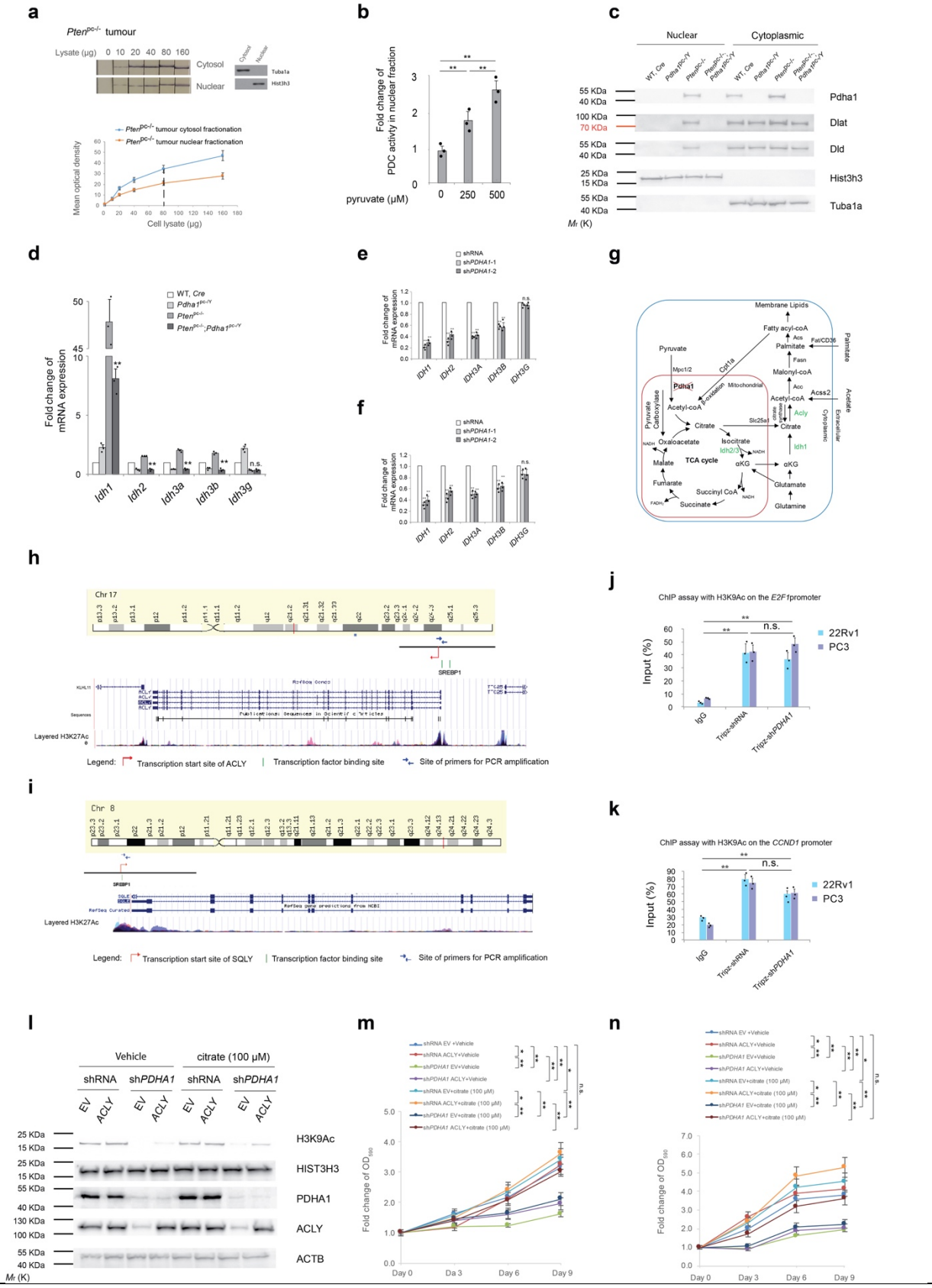

Supplementary Figure 5

PDC controls histone acetylation and the expression of genes that link reductive carboxylation to lipogenesis.

(**a**) Upper left panel, PDC activity measurements of nuclear and cytoplasmic fractions of *Pten*$^{pc-/-}$ tumours loaded in different amount in standard dipstick assay. Upper right panel, fractionation was validated by western blot analysis for the indicated proteins. Lower panel, quantification of the optical density of dipstick bands from the upper left panel. The dash line represents the amount of lysate (80 μg) used in all the measurements performed in the paper, which fall in the linear range of the assay (n=3, independent prostate samples). Uncropped images are in Supplementary Figure 14. (**b**) PDC activity measurements in nuclear fractions of *Pten*$^{pc-/-}$ tumour cells incubated in presence of pyruvate at the indicated concentration in the activity buffer (n=3, independent prostate samples). (**c**) Western blot analysis of indicated proteins in nuclear and cytoplasmic fractions in wild type, *Pdha1*$^{pc-/Y}$, *Pten*$^{pc-/-}$ and *Pten*$^{pc-/-}$; *Pdha1*$^{pc-/Y}$ prostates and tumours (n=3, independent prostate samples). Uncropped images are in Supplementary Figure 14. (**d-f**) Quantitative real time-PCR analysis of mRNA expression for Isocitrate dehydrogenase isozymes in mouse prostate tissues of indicated genotypes (n=3, independent prostate samples) (**d**) and 22Rv1(**e**) and PC3(**f**) cells infected with sh*PDHA1* or scramble shRNA control (n=3, independent cell cultures). (**g**) Schematic overview of Pyruvate dehydrogenase, tricarboxylic acid cycle, β-oxidation, glutaminolysis and lipogenesis pathways (The green represents down-regulated genes). (**h,i**) Schematic overview of primer sites of for H3K9Ac and the binding of SREBP1 detection on the *ACLY* (**h**) and *SQLE* (**i**) promoters. H3K27Ac profile (UCSC Genome Browser on Human Feb. 2009 (GRCh37/hg19) Assembly) was used for prediction of H3K9Ac status. (**j,k**) Chromatin immunoprecipitation analysis of H3K9Ac levels on the promoter of *E2F1* (**j**) and *CCND1* (**k**) in 22Rv1 and PC3 cells infected with doxycycline-induced Tripz-sh*PDHA1* or scramble control (n=3, independent cell cultures). (**l**) Western blot analysis of indicated proteins in sh*PDHA1* or scramble control 22Rv1 cells infected with ACLY over-expressing lentivirus vector or empty vector control (EV) and treated with 100 μM citrate or vehicle over a 9-day period. Uncropped images are in Supplementary Figure 15. (n=3, independent cell cultures). (**m**,**n**) Relative cell number quantification by crystal violet staining of sh*PDHA1* or scramble control 22Rv1 (**m**) and PC3 (**n**) cells infected with ACLY over-expressing lentivirus vector or empty vector control (EV) and treated with 100 μM citrate or vehicle over a 9-day period (n=3, independent cell cultures). Error bars indicate s.e.m. **P* < 0.05; ***P* < 0.01; n.s, not significant.

Supplementary Fig. 6

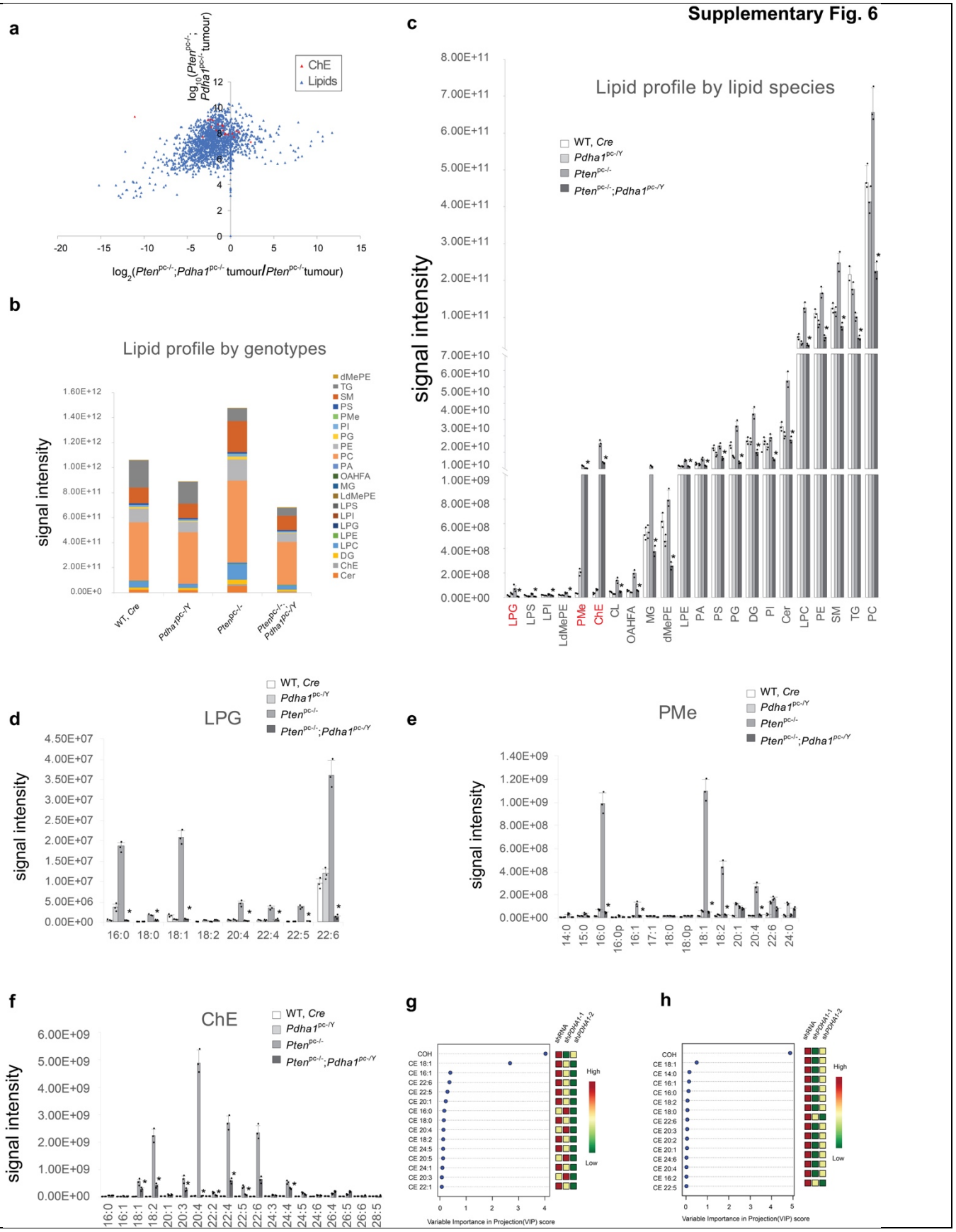

Supplementary Figure 6

PDC inactivation reduces lipid and cholesterol levels in prostate cancer.

(**a**) A scatterplot Log_{10} intensity of *Pten*$^{pc-/-}$; *Pdha1*$^{pc-/Y}$ tumours vs. Log_2 Ratio of *Pten*$^{pc-/-}$; *Pdha1*$^{pc-/Y}$ tumours versus *Pten*$^{pc-/-}$ tumours showing the distribution of 2,062 identified lipid ions (blue dots) including cholesterol esters (red dots) via LipidSearch from lipids extracted from three biological replicates of *Pten*$^{pc-/-}$; *Pdha1*$^{pc-/Y}$ tumours and *Pten*$^{pc-/-}$ tumours tissue extracts (~5 mg injected). ChE represents Cholesteryl esters (n=3, independent prostate samples) (**b,c**) The relative abundance of lipid species by intensity in wild type, *Pdha1*$^{pc-/Y}$, *Pten*$^{pc-/-}$ and *Pten*$^{pc-/-}$; *Pdha1*$^{pc-/Y}$ prostates and tumours (n=3, independent prostate samples). The top three lipids in fold change between *Pten*$^{pc-/-}$ tumours and wild type prostate were labeled as red. The lipid classes and abbreviations: Ceramide (Cer), Cholesteryl ester (ChE), Diradylglycerolipids (DG), lysophosphatidylcholine (LPC), lysophosphatidylethanolamine (LPE), lysylphosphatidylglycerol (LPG), lysophosphatidylinositol (LPI), lysophosphatidylserine (LPS), lysodimethylphosphatidylethanolamine (LdMeP), Monoradylglycerolipids (MG), (O-acyl)-omega-hydroxy fatty acids (OAHFA), phosphatidic acid (PA), phosphatidylcholine (PC), phosphatidylethanolamine (PE), Phosphatidylglycerol (PG), phosphatidylinositol (PI), phosphomonoesters (PMe), phosphatidylserine (PS), Sphingomyelin (SM), Triglyceride (TG), dimethylphosphatidylethanolamine (dMePE). (**d-f**) The relative abundance of lysylphosphatidylglycerol (LPG) (**d**), phosphomonoesters (PMe) (**e**), Cholesteryl ester (ChE) (**f**) species in wild type, *Pdha1*$^{pc-/Y}$, *Pten*$^{pc-/-}$ and *Pten*$^{pc-/-}$; *Pdha1*$^{pc-/Y}$ prostates and tumours (n=3, independent prostate samples). (**g,h**) Significantly changed levels of cholesterol (COH) and 14 Cholesteryl esters (CE) in 22Rv1 (**g**) and PC3 (**h**) cells infected with two sh*PDHA1* or a scramble shRNA control (n=3, independent cell cultures). The Variable Importance in Projection (VIP) scores depicting the top-ranked metabolites that contributed to the separation of prostate cancer cells infected with two sh*PDHA1* and a scramble control. A value of VIP score greater than 1 suggests actual contribution of the considered lipid to the group separation. The coloured boxes on the right indicate the relative concentrations of the corresponding metabolite in each group under study. The scale bar depicts the relative metabolite levels (red, high abundance; blue, low abundance). Error bars indicate s.e.m. *$P < 0.05$; n.s, not significant.

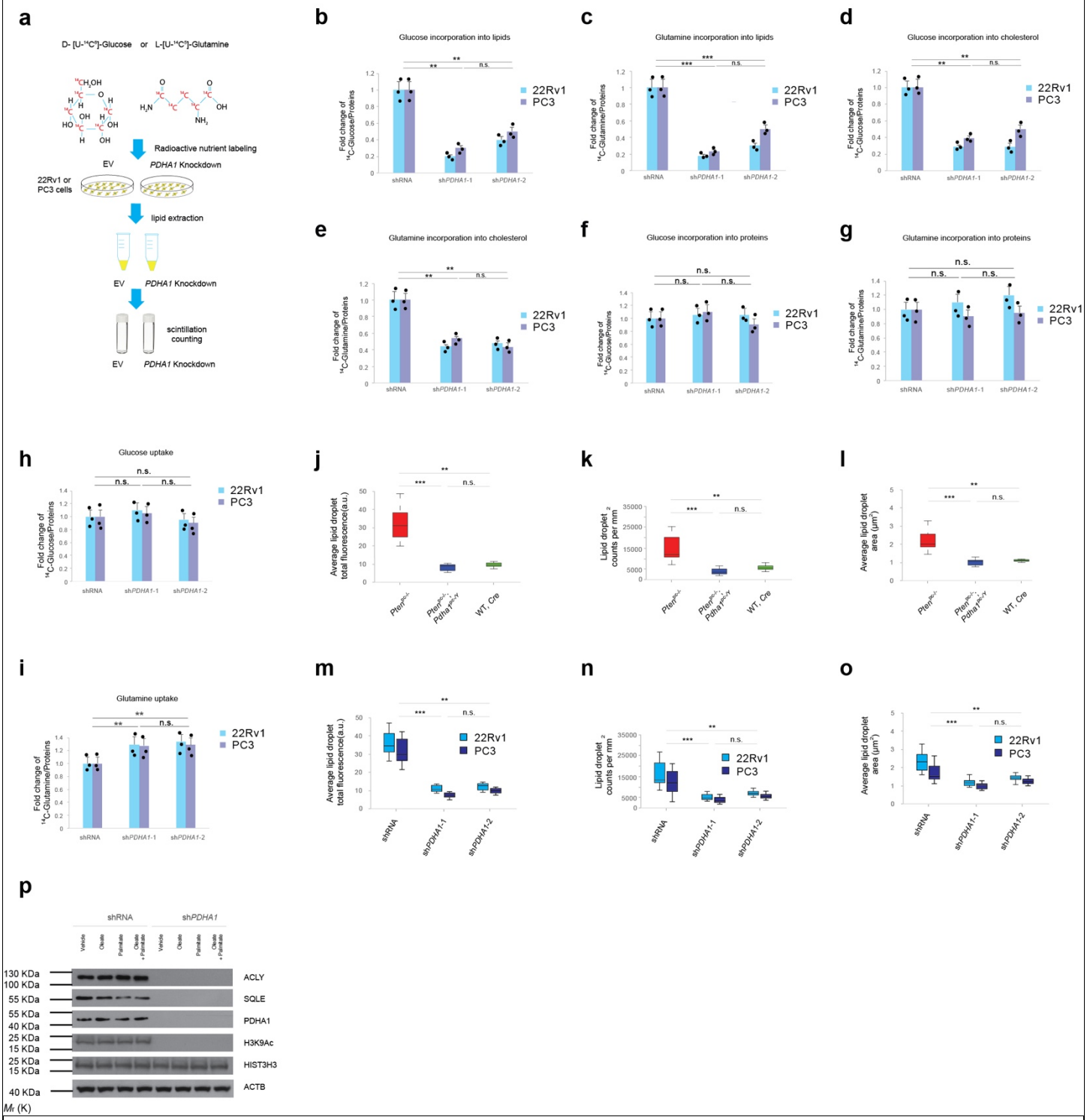

Supplementary Figure 7

***Pdha1* inactivation mainly affects de novo lipid synthesis in prostate cancer.**

(**a**) Scheme of radioactive ^{14}C tracing using D- [U-$^{14}C_6$]-Glucose (^{14}C-Glucose) and L-[U-$^{14}C_5$]-Glutamine (^{14}C-Glutamine) measuring glucose and glutamine incorporation into lipids. (**b,c**) Radioactive tracing using ^{14}C-glucose (**b**) and ^{14}C-glutamine (**c**) for *de novo* lipogenesis in 22Rv1 and PC3 cells infected with two sh*PDHA1* and scramble shRNA control (n=3, independent cell cultures). (**d,e**) Radioactive tracing using ^{14}C- glucose (**d**) and ^{14}C-glutamine (**e**) for *de novo* cholesterol synthesis in 22Rv1 and PC3 cells infected with two sh*PDHA1* and scramble shRNA control (n=3, independent cell cultures). (**f,g**)Radioactive tracing using ^{14}C- glucose (**d**) and ^{14}C-glutamine (**e**) in protein synthesis in 22Rv1 and PC3 prostate cancer cell line infected with sh*PDHA1* or scramble shRNA control (n=3, independent cell cultures). (**h,i**) Glucose uptake (**h**) and glutamine uptake (**i**) analysis in 22Rv1 and PC3 cells infected with sh*PDHA1* or scramble shRNA control (n=3, independent cell cultures). (**j-l**) Confocal microscopy quantification of intra-tumour lipid droplets by average lipid droplets total fluorescence (a.u.) (**j**) average lipid droplets per mm^2 (**k**) and average lipid droplet area in μm^2 (**l**) in the indicated genotypes (n=3 independent prostate samples, 5 fields acquired for each group) in *Pten*$^{pc-/-}$; *Pdha1*$^{pc-/Y}$ versus *Pten*$^{pc-/-}$ prostate tumours. DAPI, blue. Scale bar: 20 μm (n=3 independent prostate samples, 5 fields acquired). (**m-o**) Confocal microscopy quantification of intra-tumour lipid droplets by average lipid droplet total fluorescence (a.u.) (**m**) average lipid droplets per mm^2 (**n**) and average lipid droplet area in μm^2 (**o**) in 22Rv1 and PC3 sh*PDHA1* and shRNA xenograft tumours. DAPI, blue. (n=3, independent prostate samples, 5 fields acquired and scale bar represents 20 μm). (**p**) Western blot analysis of indicated proteins in 22Rv1 cells infected with sh*PDHA1* or scramble control and treated with exogenous fatty acids in fatty acid-free media; oleate (25μM), palmitate (25 μM) or a combination of these two over a 6-day period. Uncropped images are in Supplementary Figure 15. (n=3, independent cell cultures). Error bars indicate s.e.m. $^{**}P < 0.01$; $^{***}P < 0.001$. n.s, not significant.

Supplementary Fig. 8

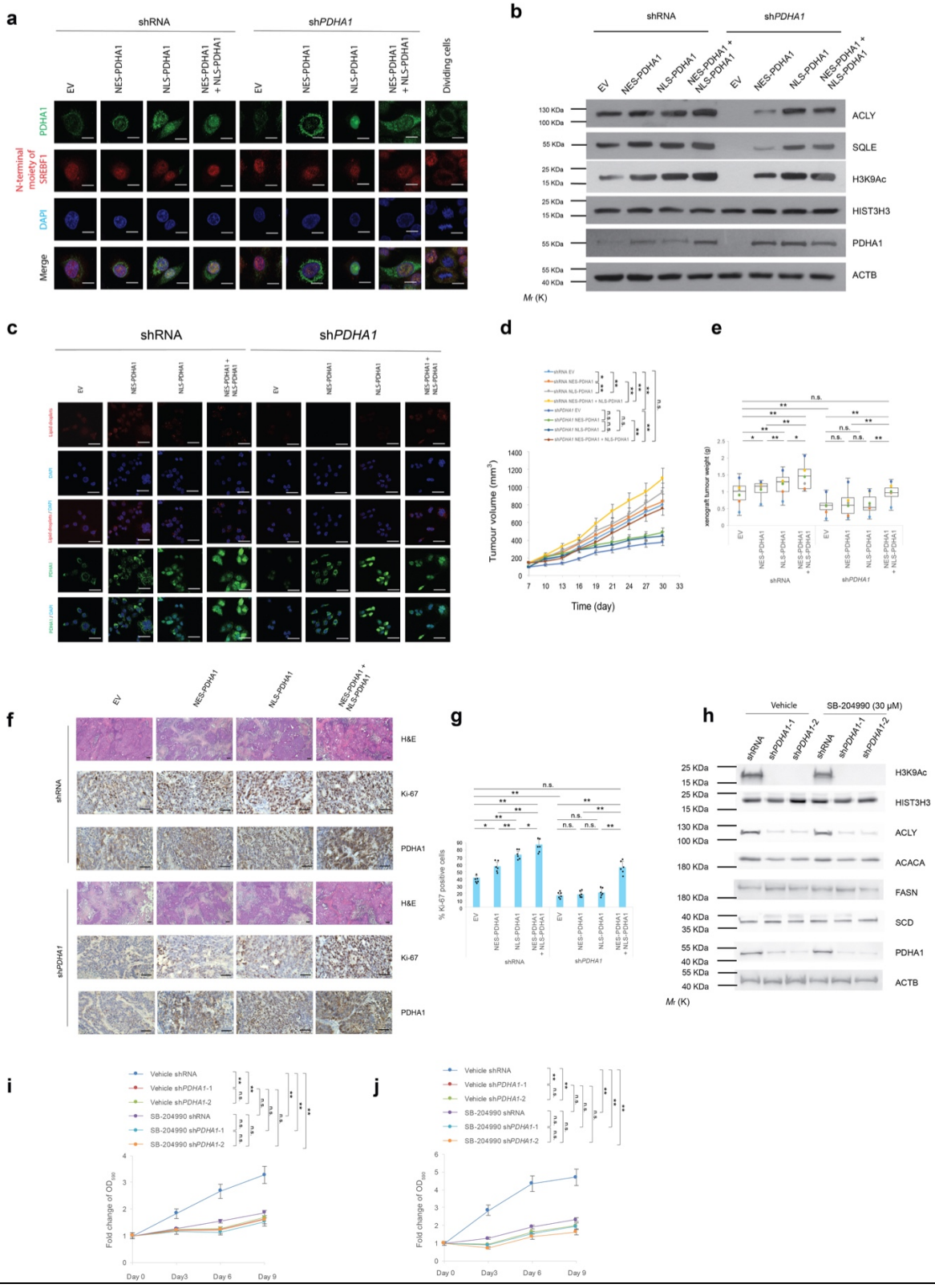

Supplementary Figure 8

Both nuclear PDC and mitochondrial PDC are required for prostate cancer cell proliferation.

(**a-g**) Representative images of confocal microscopy for PDHA1 and the N-terminus mature form of SREBF1 (n=3, independent cell cultures, 5 fields acquired for each group and scale bar represents 10 μm) (**a**), western blot analysis of indicated proteins (n=3) (**b**), representative images of PDHA1 and lipid droplets in confocal microscopy. Uncropped images are in Supplementary Figure 15. (n=3, independent cell cultures, 5 fields acquired for each group and scale bar represents 50 μm) (**c**), evaluation of tumour formation in xenotransplantation experiments (n=6, independent tumour samples) (**d**), tumour mass in xenotransplantation experiments (n=6, independent tumour samples) (**e**), representative micrographs in histopathological analysis (haematoxylin/eosin staining and indicated proteins) in xenotransplantation experiments (n=6, independent tumour samples, 5 fields acquired for each group and scale bar represents 50 μm) (**f**) and quantification of the percentage of Ki-67 positive cells in xenotransplantation experiments (n=6, independent tumour samples) (**g**) of sh*PDHA1* or shRNA control 22Rv1 cells infected with NES-PDHA1, NLS-PDHA1 alone or in combination. (**h**) Western blot analysis of indicated proteins in the 22Rv1 cells infected with two shPDHA1 and a scramble shRNA control and treated with SB-204990, a selective ACLY inhibitors at the dose of 30 μM which effectively arrest cell growth as shown in panel (**i**) in this figure or vehicle for 9 days (n=3, independent cell cultures). Uncropped images are in Supplementary Figure 15. (**i**,**j**) the relative cell number quantification of the 22Rv1 cells (**i**) and PC3 cells (**j**) infected with two shPDHA1 and a scramble shRNA control and treated with SB-204990, a selective ACLY inhibitors at the dose of 30 μM for 9 days (n=3, independent cell cultures). Error bars indicate s.e.m. *$P < 0.05$; **$P < 0.01$. n.s, not significant.

Supplementary Fig. 9

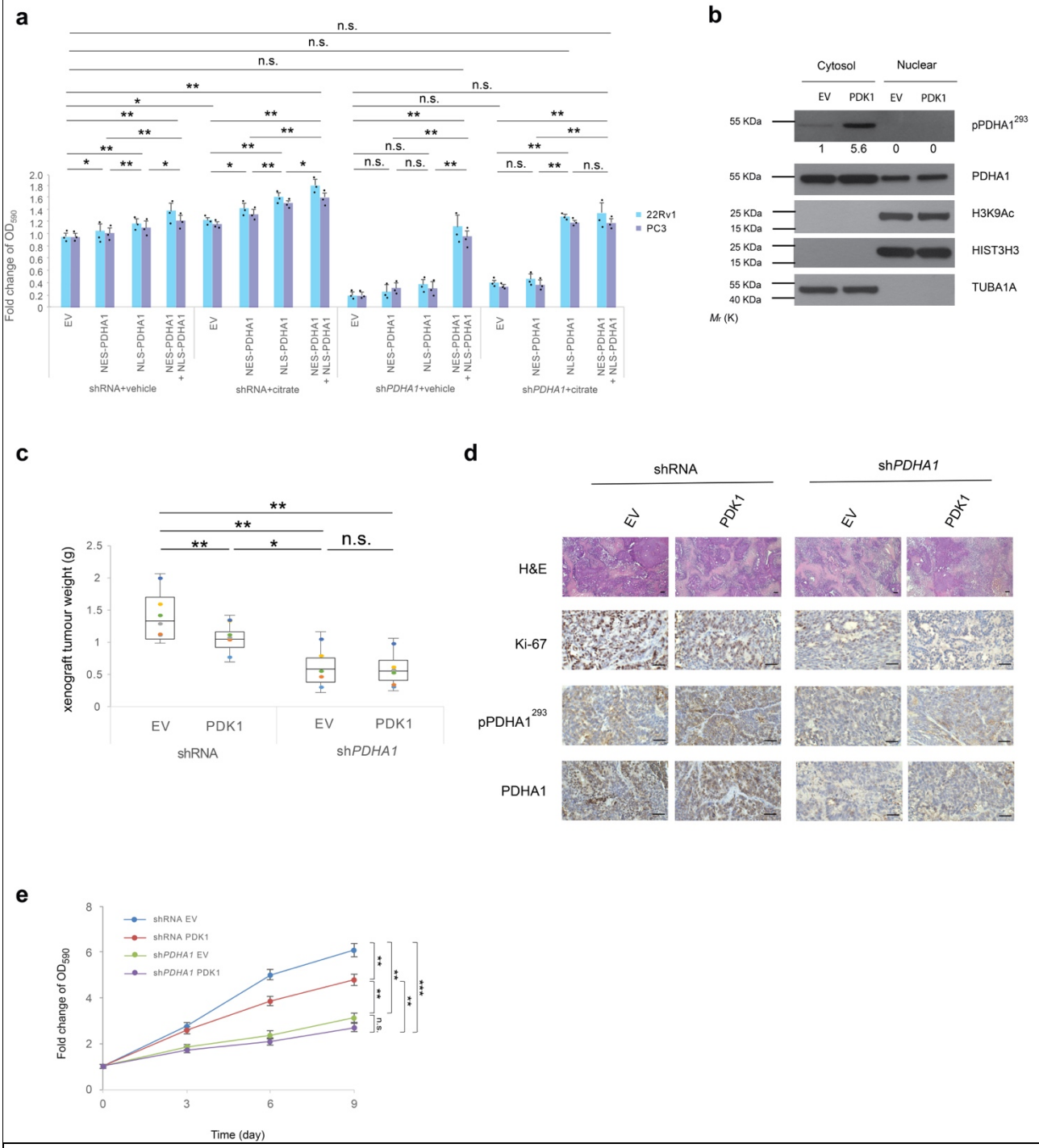

Supplementary Figure 9

Mitochondrial PDC inhibition compromises prostate cancer cell proliferation by reducing citrate production.

(**a**) Relative cell number quantification by crystal violet staining of sh*PDHA1* or shRNA control 22Rv1 or PC3 cells infected with NES-PDHA1 and NLS-PDHA1 alone or in combination and treated with citrate (100 μM) or vehicle (n=3, independent cell cultures). (**b**) Western blot analysis of indicated proteins in nuclear and cytoplasmic fractions in 22Rv1 cells infected with PDK1 or empty vector control. Uncropped images are in Supplementary Figure 15. (n=3, independent cell cultures) (**c-e**) Tumour mass in xenotransplantation experiments (n=6, independent tumour samples) (**c**), representative micrographs in histopathological analysis (haematoxylin/eosin staining and indicated proteins) (n=6, independent tumour samples and scale bar represents 50 μm) (**d**) and relative cell number quantification by crystal violet (n=3, independent cell cultures) (**e**) of sh*PDHA1* or shRNA control 22Rv1 cells infected with PDK1 or empty vector control. Error bars indicate s.e.m. *$P < 0.05$; **$P < 0.01$; ***$P < 0.001$. n.s, not significant.

Supplementary Fig. 10

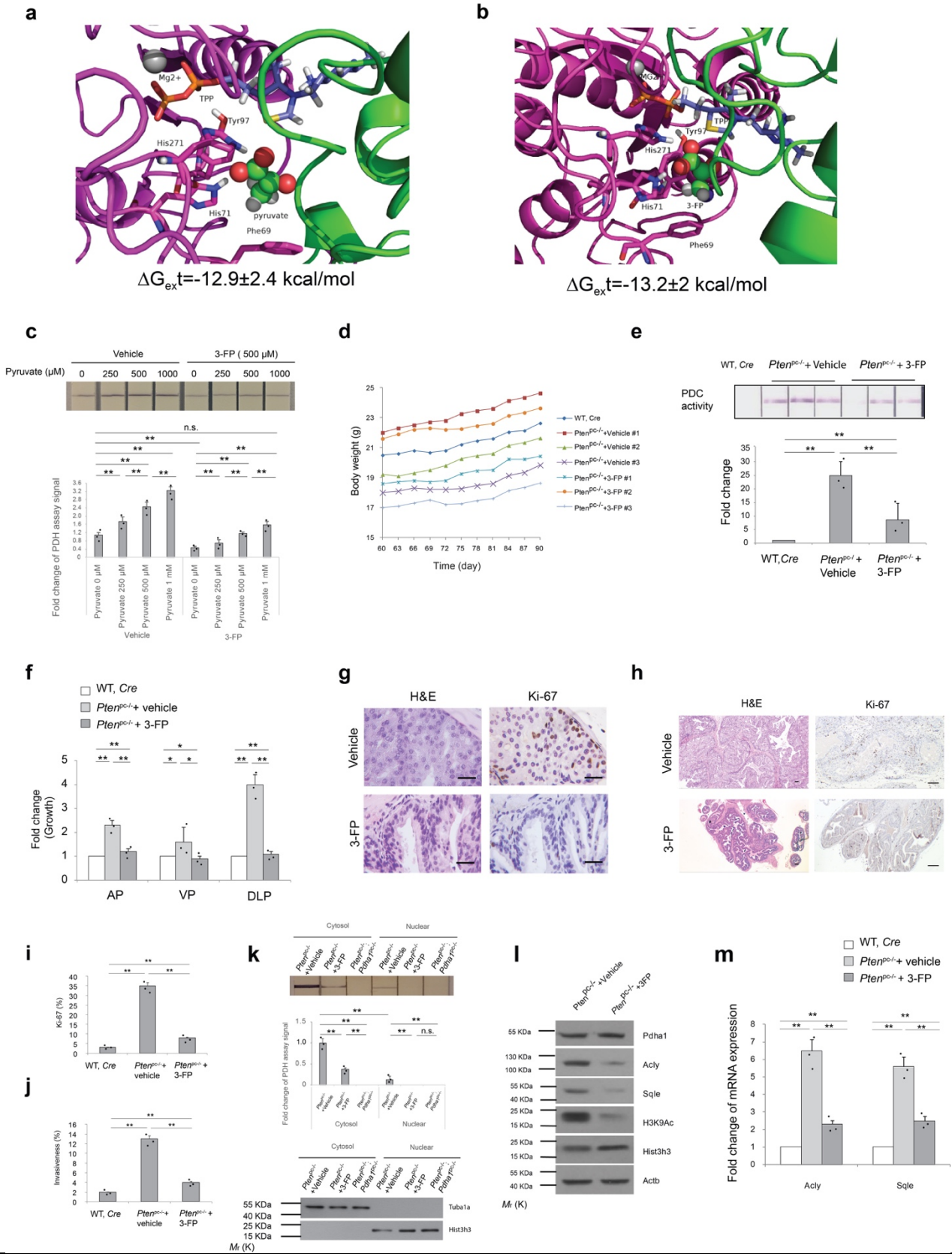

Supplementary Figure 10

Pharmacological inhibition of PDHA1 arrests mouse and human prostate tumours.

(**a,b**) Representative structures, selected from MD simulations of the PDHA1/pyruvate (**a**) and PDHA1/3-FP (**b**) complexes. The a and b chains are represented as magenta and green ribbons, respectively. In the picture of PDHA1/3-FP complex, the fluorine atom is depicted in violet. Binding Delta G values, estimated by MM-GBSA, are also reported. (**c**) Upper panel, PDC activity measurements in the lysate from 22Rv1 cells treated with 3-FP or vehicle and supplemented with indicated amount of pyruvate in activity buffer of dipstick assay kit (n=3, independent cell cultures). Lower panel, quantification of PDC activity by mean optical density of colored bands shown on dipsticks in upper panel (n=3, independent cell cultures). (**d**) Body weight of mice of the indicated genotypes treated with 3-FP or vehicle from 8 weeks old for one month (n=3, independent mice). (**e**) Upper panel, PDC activity measurements, and quantification in anterior prostate of indicated genotypes from mice treated with 3-FP or vehicle from 8 weeks old for one month (n=3, independent prostate samples). Lower panel, quantification of PDC activity by mean optical density of colored bands shown on dipsticks in upper panel (n=3, independent prostate samples). (**f**) Comparison of prostate lobe volumes from male mice at age of 12 weeks treated with 3-FP or vehicle for one month (mm^3, 2 independent lobes per animal are presented. AP, anterior prostate; VP, ventral prostate; DLP, dorsal and lateral prostate, n=3, independent prostate samples). (**g-j**) Representative micrographs of histopathological analysis (haematoxylin/eosin and Ki-67 staining) of anterior prostates (AP) in *Pten*$^{pc-/-}$ prostate tumours (n=3, independent prostate samples, 5 fields, and scale bar represents 50 μm) (**g,h**), quantification of the percentage of Ki-67 positive cells (n=3 independent prostate samples, 5 fields) (**i**) and quantification of the percentage of invasive prostate cancer glands in *Pten*$^{pc-/-}$ prostate tissue (n=3, independent prostate samples, 5 fields) (**j**) from male mice at age of 8 weeks treated with 3-FP or vehicle for one month. (**k**) Upper panel, PDC activity measurements and quantification in nuclear and cytoplasmic fractions of prostate tumours of indicated genotypes from mice at age of 8 weeks treated with 3-FP or vehicle for one month (n=3, independent prostate samples). Lower panel, fractionation was validated by western blot analysis for the indicated nuclear and cytosolic proteins. Uncropped images are in Supplementary Figure 15. (**l**) Western blot analysis of indicated proteins in prostate tumours from *Pten*$^{pc-/-}$ mice at age of 8 weeks treated with 3-FP or vehicle for one month (n=3, independent prostate samples). (**m**) Quantitative real time-PCR analysis of mRNA expression for *Acly* and *Sqle* from mice of indicated genotypes at age of 8 weeks treated with 3-FP or vehicle for one month (n=3, independent prostate samples). Error bars indicate s.e.m. *$P < 0.05$; **$P < 0.01$. n.s, not significant.

Supplementary Fig. 11

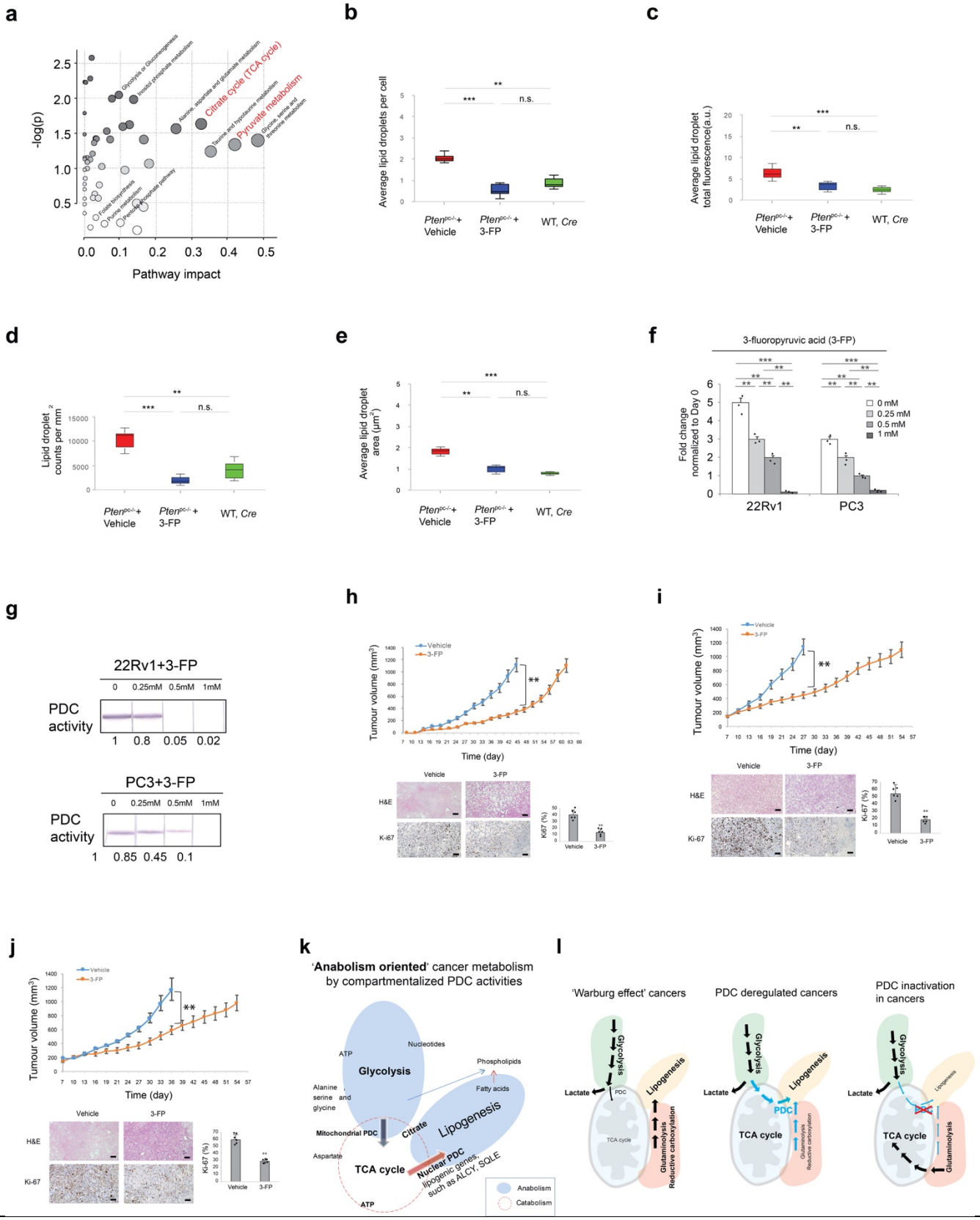

Supplementary Figure 11

Pharmacological inhibition of PDHA1 arrests mouse and human prostate tumours.

(**a**) Integrating enrichment analysis and pathway topology analysis of metabolic pathways in prostate tumours from *Pten*$^{pc-/-}$ mice at age of 8 weeks treated with or without 3-FP for one month (n=3, independent prostate samples). (**b-e**) Quantification of confocal microscopy for lipid droplets (Lipidtox; red) by lipid droplet counts per cell (**b**), average lipid droplets fluorescence (a.u) (**c**), lipid droplet counts per mm^2 (**d**), average lipid droplets area in μm^2 (**e**) in wild type and *Pten*$^{pc-/-}$ prostate tissues from 8 weeks old male mice treated with 3-FP or vehicle for one month (n=3, independent prostate samples, 5 fields). (**f,g**) Relative cell number quantification by crystal violet staining (**f**) and PDC activity measurements (**g**) in indicated prostate cancer cell lines treated with 3-fluoropyruvic acid (3-FP) at the indicated concentration for 6 days (n=3, independent cell cultures). (**h-j**) Evaluation of tumour formation and quantification of the percentage of Ki-67 positive cells in xenotransplantation experiment in LNCaP (**h**), 22Rv1 (**i**) and PC3 (**j**) cells treated with 3-FP or vehicle for two months (n=6, independent tumour samples, 5 fields and scale bar represents 50 μm). (**k**) Schematic representation of the role of mitochondrial and nuclear PDH complex functions in regulating glucose influx of TCA cycle and controlling the diversion of TCA cycle intermediates (or glutamine derived anaplerosis pathway) into lipogenesis. (**l**) Metabolic landscape describing the functional relevance of PDC complex in regulating non-canonical tumour metabolism. Contrast to classic 'Warburg effect' where cancers rely predominantly on glycolysis and catabolic TCA cycle gets restrained, tumours could achieve another 'anabolism oriented' reprogramming/axis by upregulating PDC and promoting PDC nuclear translocation. Nuclear PDC controls the transitory process in TCA cycle by allowing the short-lived entry and exit of carbon pool in mitochondria to fuel citrate synthesis and lipogenesis. Taking advantage of this diversion caused by nuclear PDC, the tumour cells reduce carbon consumption in TCA cycle thereby benefiting proliferation. PDC inactivation arrests nuclear PDC active cancers by abrogating both glucose influx and potential anaplerosis pathways from reductive carboxylation and glutaminolysis. The blue represents the pathways controlled by PDC. Error bars indicate s.e.m. $^{**}P < 0.01$; $^{***}P < 0.001$. n.s, not significant.

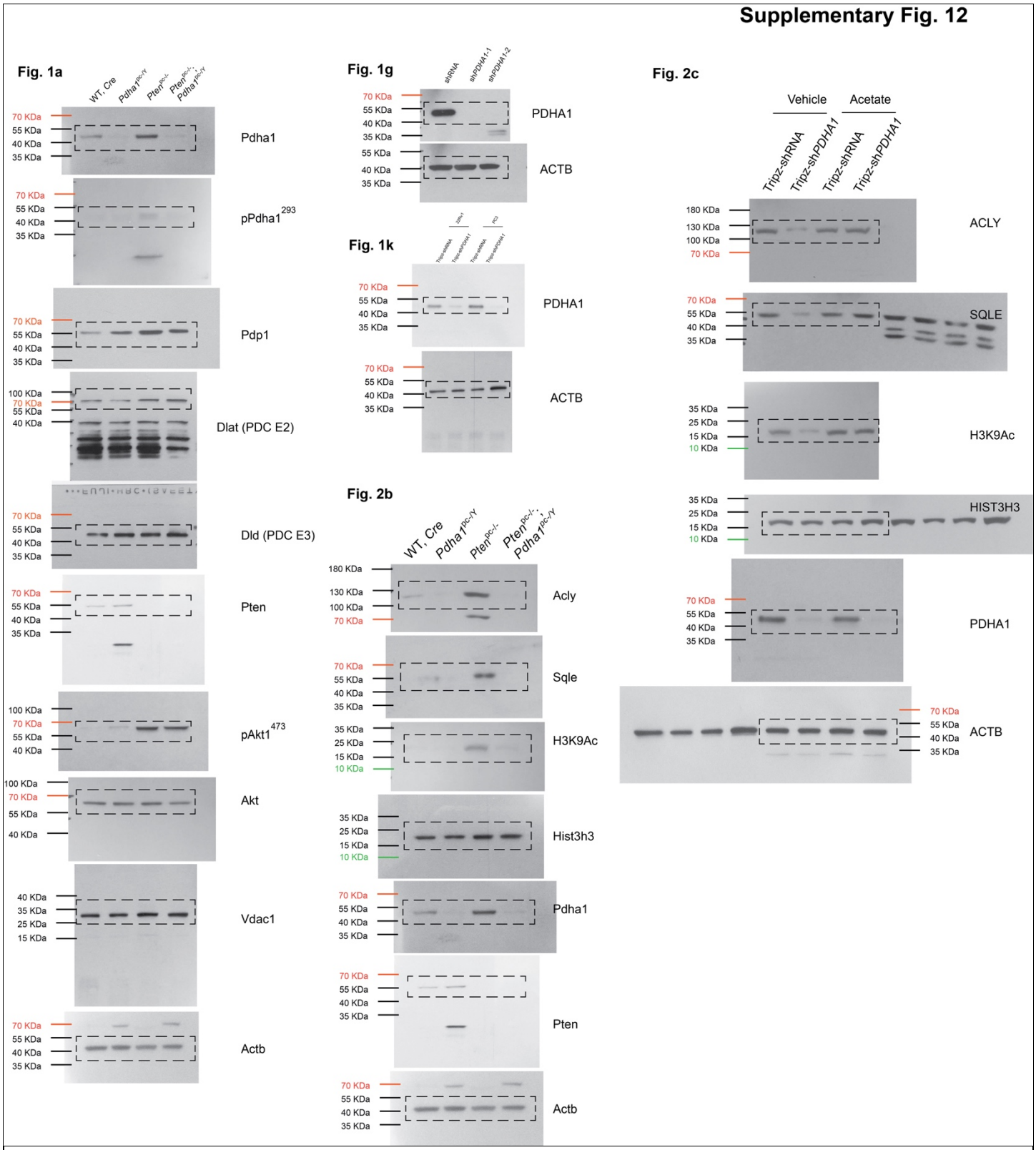

Supplementary Figure 12

Uncropped full-length pictures of Western blotting membranes presented in the main Fig. 1a, 1g, 1k, 2b and 2c
Membranes were often cut to enable blotting for multiple antibodies

Supplementary Fig. 13

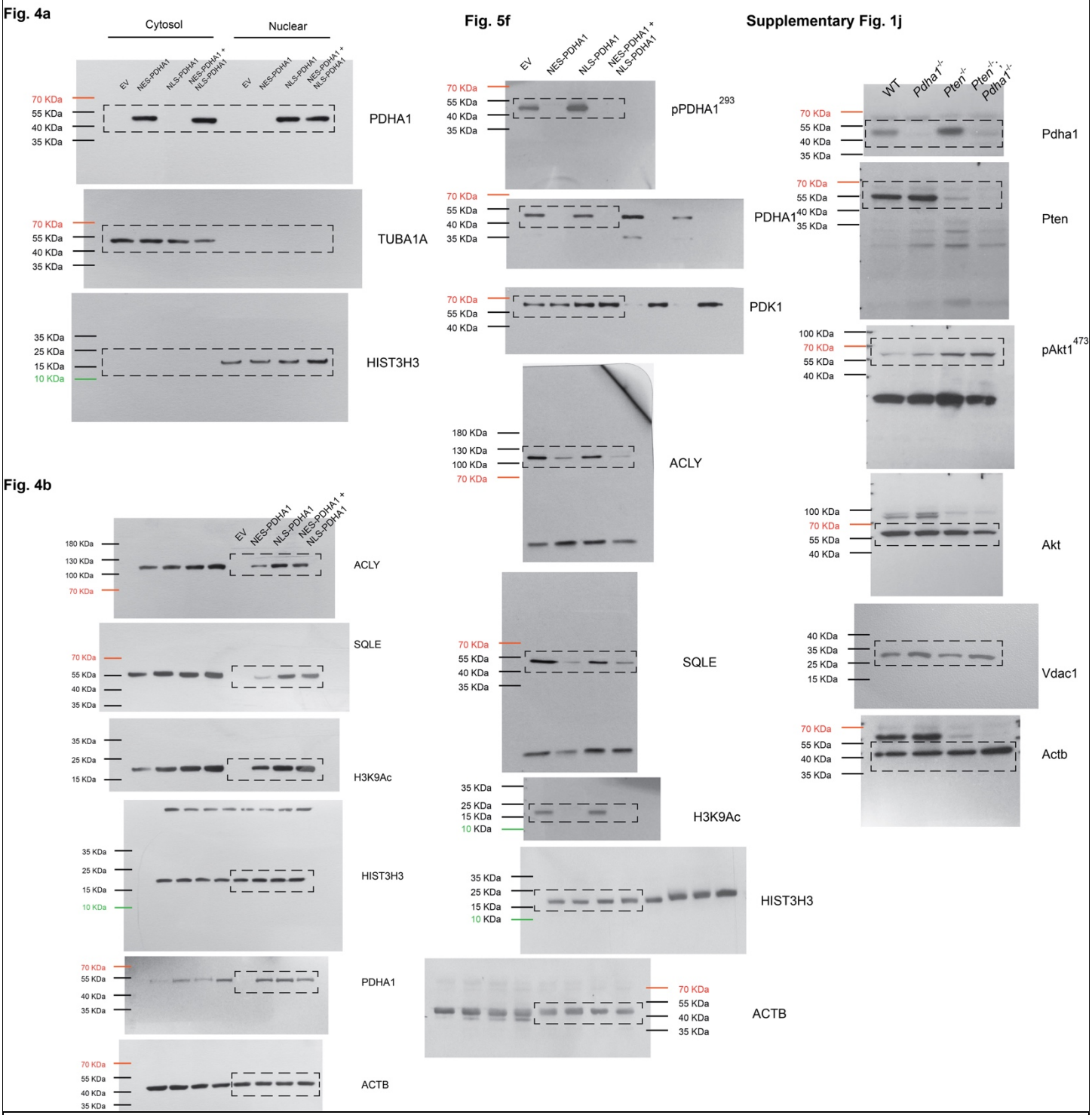

Supplementary Figure 13

Uncropped full-length pictures of Western blotting membranes presented in the main Fig. 4a, 4b, 5f and Supplementary Fig. 1j
Membranes were often cut to enable blotting for multiple antibodies

Supplementary Fig. 14

Supplementary Fig. 3f

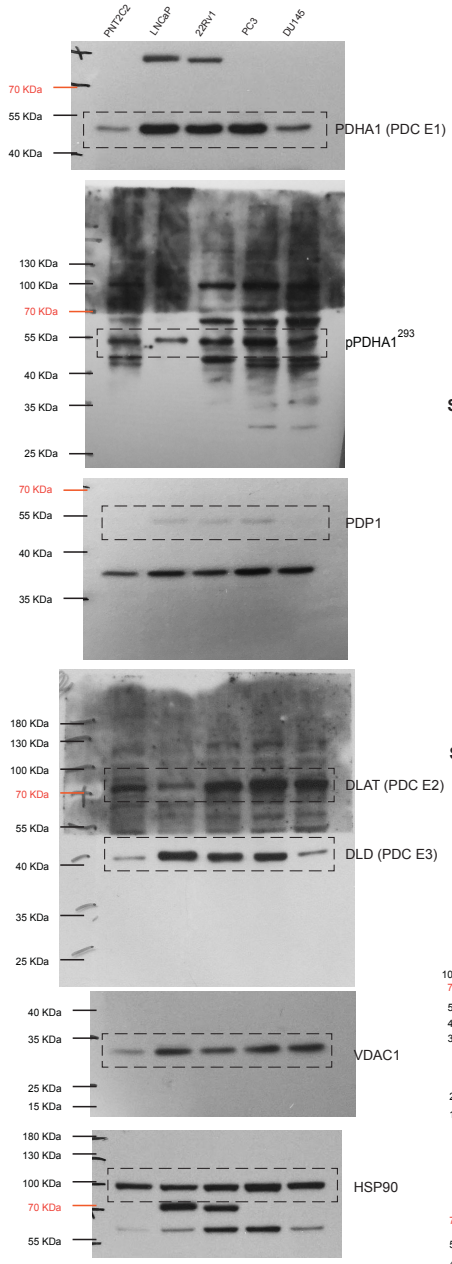

Supplementary Fig. 3m

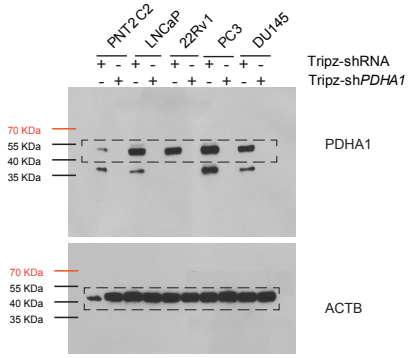

Supplementary Fig. 5a

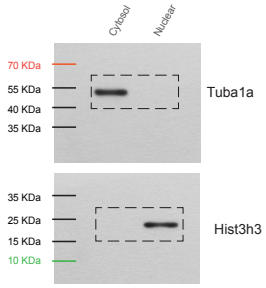

Supplementary Fig. 5c

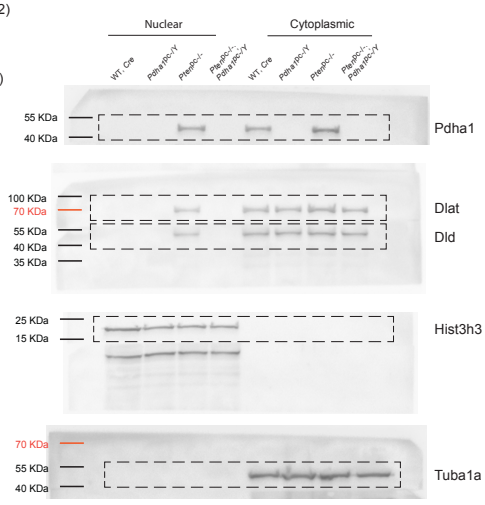

Supplementary Figure 14

Uncropped full-length pictures of Western blotting membranes presented in the Supplementary Fig. 3f, 3m, 5a and 5c

Membranes were often cut to enable blotting for multiple antibodies

Supplementary Fig. 15

Supplementary Fig. 5l

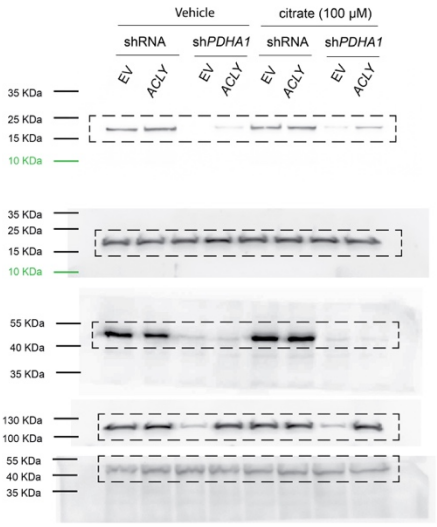

Supplementary Fig. 8b

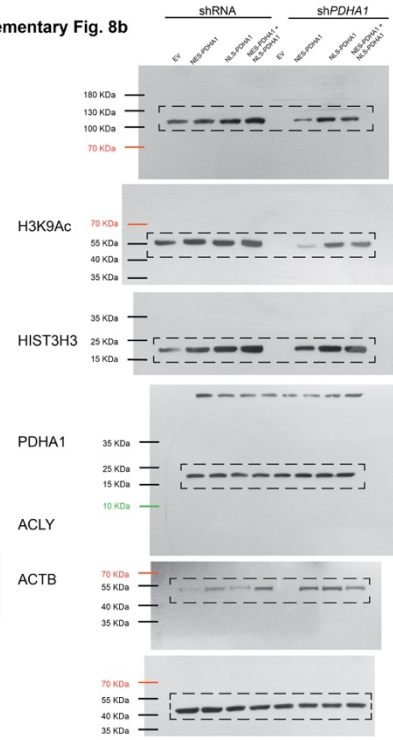

Supplementary Fig. 9b

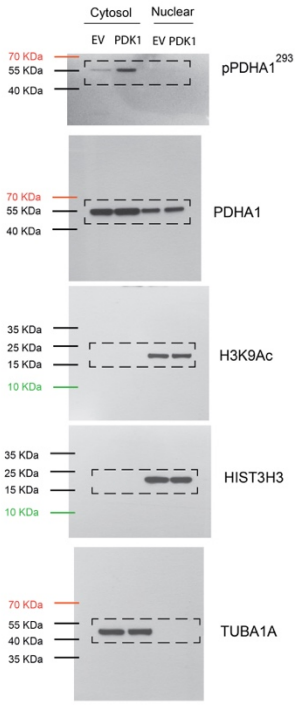

Supplementary Fig. 7p

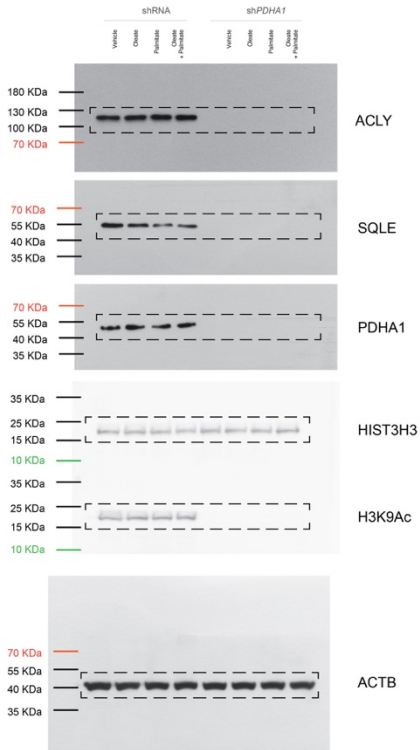

Supplementary Fig. 8h

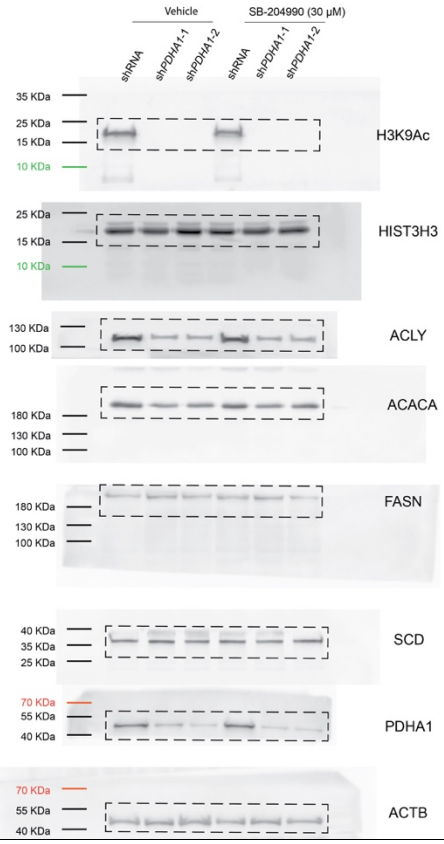

Supplementary Fig. 10k

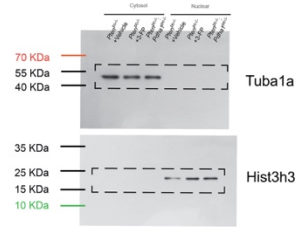

Supplementary Figure 15

Uncropped full-length pictures of Western blotting membranes presented in the Supplementary Fig. 5l, 7p, 8b, 8h, 9b and 10k

Membranes were often cut to enable blotting for multiple antibodies